International Journal of
Clinical Cardiology & Research

Research Article

Unsteady LDL Transport through Patient-Specific Multi-Layer Left Coronary Artery -

Dimitrios G. Mpairaktaris[1]*, Johannes V. Soulis[1#] and George D. Giannoglou[2#]

[1]Fluid Mechanics Division, School of Engineering, Democritus University of Thrace, Xanthi, Greece
[2]Cardiovascular Engineering and Atherosclerosis Laboratory, 1st Cardiology Department, AHEPA University; Hospital, Medical School, Aristotle University of Thessaloniki, Thessaloniki, Greece
[#]These authors contributed equally to this work

***Address for Correspondence:** Dimitrios G. Mpairaktaris, Fluid Mechanics Division, Faculty of Engineering, Democritus University of Thrace, Vas. Sofias 12, 67100 Xanthi, Greece, Tel: +302-541-079-617; E-mail: dmpaira@gmail.com; ORCID ID: orcid.org/0000-0002-3889-8747

Submitted: 23 May 2018; **Approved:** 22 June 2018; **Published:** 25 June 2018

Cite this article: Mpairaktaris DG, Soulis JV, Giannoglou GD. Unsteady LDL Transport through Patient-Specific Multi-Layer Left Coronary Artery. Int J Clin Cardiol Res. 2018;2(2): 039-049.

ISSN: 2639-3786

ISSN: 2639-3786

ABSTRACT

Aims: The objective of the study is to study the transport and distribution of Low Density Lipoprotein (LDL) within patient-specific multi-layer arterial wall model under unsteady flow using computational fluid dynamic analysis.

Methods: A Left Coronary Artery (LCA) patient-specific model was incorporated. Both flow-mass transport equations in lumen as well as flow-mass transport equations within the patient-specific multi-layer arterial wall are numerically analyzed.

Results: The lumen-side LDL concentration preferably occurs at the concave geometry parts denoting concentration polarization. The Average Wall Shear Stress (AWSS) is not the only factor that can determine the lumen-side concentration of LDL. Increased time-averaged luminal concentration develops mainly in the proximal rather than to distal segment flow parts. The LDL concentration at the endothelium/intima interface is substantially lower, almost 90 times, than its value at lumen/endothelium interface. The concentration drop across the intima layer is negligible, whereas the concentration reduction across the Internal Elastic Layer (IEL) is remarkable. LDL concentration values at the IEL/media interface are one order of magnitude smaller to ones occurring at the intima layer.

Conclusions: The transportation of LDL through the multi-layer arterial wall is affected by the flow pattern itself, the arterial wall thickness and the physical values of the layers.

Keywords: Patient-specific; Left coronary artery; Multi-layer arterial wall; Low density lipoprotein transport; Atherosclerosis

NOMENCLATURE

C: concentration (gr/l); $\overline{C}$: average concentration gr/l; D: diffusivity (m^2/s); D' : diffusivity per unit length (m/s); Δp: pressure drop (N/m^2); J: flux (m/s); K: permeability (m^2); K': solute lag; L: hydraulic conductivity (m^2 s/gr); L": thickness (m); R: radial location from the centerline (m); p: pressure (N/m^2); r: constant consumption rate; u: velocity (m/s)

SUBSCRIPTS

l: lumen; lag: coefficient; o: inlet; p: plasma; s: solute; v: volume; eff: effective property; w: wall; in: instantaneous

SUPERSCRIPTS

end: endothelium; in: intima; iel: internal elastic layer; m: media

GREEK SYMBOLS

μ: molecular viscosity (Pa s); σ_d: osmotic reflection coefficient of the endothelium; σ_f: solvent reflection coefficient; ρ: density (Kg/m^3); ε: porosit

INTRODUCTION

On the data basis taken from National Health and Nutrition Examination Survey (NHANES) 2009 to 2012, an estimated 15.5 million Americans over 20 years of age have coronary heart disease [1]. It is widely accepted that the cardiovascular disease, in general, is associated with atherosclerosis and the real causes of atherogenesis have not yet fully been established. The main risk factor for this disease is considered to be the transportation of Low Density Lipoprotein (LDL) across the arterial wall. The mechanism through which the mass is transported from lumen to the multi-layer wall needs to be elucidated.

Several studies have proved that the flow in coronary arteries is locally disturbed by the formation of complex secondary and recirculation flows. In turn, these flows create regions of very low Wall Shear Stress (WSS) [2] which are sceptical to atherosclerotic plaque growth [3-5]. However, WSS is not the only factor that determines the formation of plaque through luminal and arterial LDL accumulation [6]. Other factors, that probably affect the concentration changes at endothelium interface, are the particular flow pattern itself [6], the mechanism through which the oxidized LDL species lead to foam cell formation [7] and the different physical parameters of the arterial wall from layer to layer [7].

Numerous computational models have been applied for idealized arteries [8-18]. In spite of the great technological advances in recent years, particularly in cardiovascular imaging and computational analysis, scientists have been empowered to numerically simulate realistic arteries [7,19-21]. LDL transport through the artery wall based on idealized geometries implies that the influence of the geometry on the flow pattern is not taken into account. Henceforth, regions of low WSS cannot be properly estimated, which in turn it leads to unsatisfactory estimations of the LDL distribution at the luminal side as well as inside to the arterial wall.

It is of significant importance to assess whether unsteady, in comparison to steady flow, has an important impact on LDL transport process from lumen to multi-layer wall. The long-term LDL transport is a central processing unit time consuming process. This, in turn, increases the computational demand. However, no matter how difficult the task is, current work aims to quantify the oscillating LDL concentration and its distribution within patient-specific multi-layer arterial wall. Current flow-mass transport analysis refers to a 3D Left Coronary Artery (LCA) patient-specific segment under oscillating pulse wave form for resting flow condition. Both flow-mass transport equations in lumen as well as flow-mass transport equations within the patient-specific multi-layer arterial wall are numerically analysed.

METHODS

Acquisition of anatomy data

The LCA patient specific model was derived by the IVUS Angio tool which has been previously validated [22]. The basis for generating 3D geometry is the creation of numerous closed 3D curves using Rhinoceros 4.0 (Figure 1A & 1B). The distance between two successive curves is 0.5 mm. The length of the acquired patient-specific segment is 6.2 cm with lumen average diameter of 3.0 mm and average wall thickness of 0.24 mm. The acquired surfaces: endothelium, Internal Elastic Layer (IEL) and adventitia as well as the acquired layers: lumen, intima and media were reconstructed using ANSYS Design Modeler software.

Model construction

The reconstruction of each layer constitutes a difficult task. The acquired LCA model has variable wall thickness. Specifically,

the intima layer is comprised of constant wall thickness with 0.012 mm in order to avoid intimal hyperplasia while the media layer has variable wall thickness. The endothelium and IEL were assumed to be semi-permeable biological membranes due to the extremely low wall thickness. The constructed model was imported into appropriate software and the boundary zones were accordingly specified. A mesh sensitive study was performed to solve the fundamental flow-mass transport equations in the lumen. The mesh independence criterion was mainly based in the WSS convergence criterion satisfaction (Figure 2A & 2B). The final grid size was comprised of 586204 nodes, 491164 cells and 1567980 faces for lumen, 753732 nodes, 501984 cells and 1757448 faces for intima layer and 237742 nodes, 1061714 cells and 2245134 faces for media layer.

Flow and mass transport equations

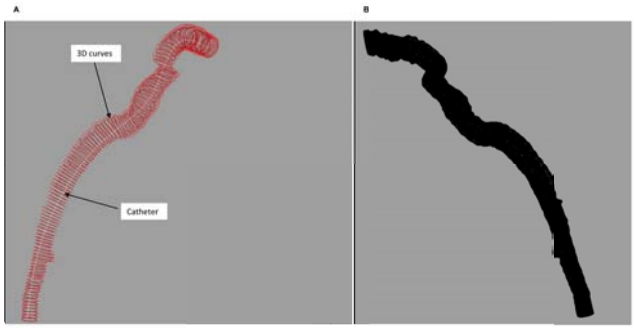

Figure 1: A. Numerous closed 3D curves are used for 3D LCA geometry generation. B. The generated geometry of the LCA segment

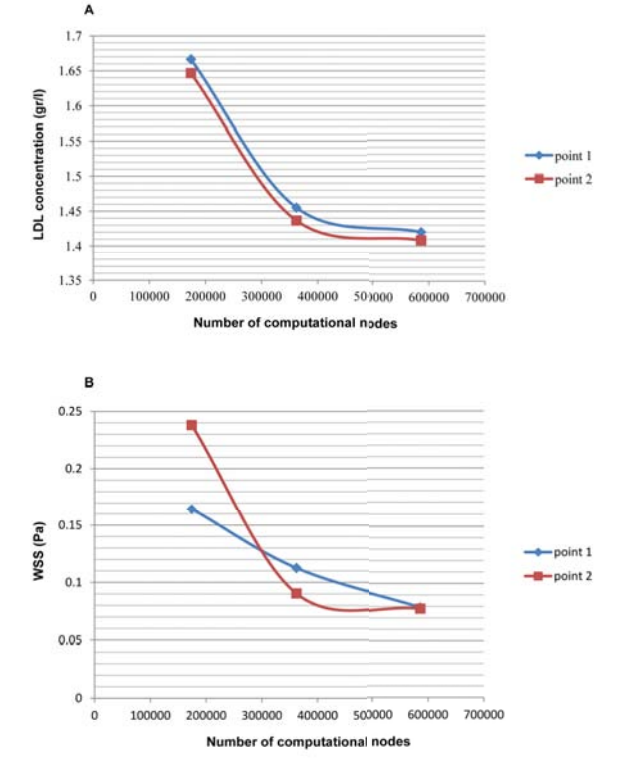

Figure 2: A. LDL concentration (gr/l) versus number of computational grid nodes for two endothelium grid node points arbitrary chosen.
B. WSS (Pa) versus number of computational grid nodes for the same grid node points.

The applied numerical code solves the governing unsteady 3D Navier-Stokes equations for lumen flow and the mass transport equation. The LCA is treated as being of non-elastic, stationary and rigid material. For calculation simplicity, an assumption has been made about the transport properties of the endothelium. This assumption states that solute endothelial permeability coefficient is not shear flow dependent. The intima and the patient-specific media layer are considered to be porous media.

Flow equations

Lumen flow: In their generality the mass flow equation for the lumen is,

$$\frac{\partial \rho}{\partial t} + \nabla \bullet \left(\rho \vec{u}_l \right) = 0 \tag{1}$$

ρ (kg/m^3) is the blood density; t (s) the time and $\vec{u}_l$ (m/s) is the lumen velocity vector. The conservation of momentum is,

$$\frac{\partial}{\partial t}\left(\rho \vec{u}_l \right) + \nabla \bullet \left(\rho \vec{u}_l \vec{u}_l \right) + \nabla p_l = \nabla \bullet \left(\bar{\tau} \right) + \rho \vec{g} \tag{2}$$

p_l (N/m^2 or Pa) is the blood static pressure within lumen; $\bar{\tau}$ (N/m^2) the shear stress tensor and $\rho \vec{g}$ (N/m^3) the gravitational body force. The shear stress tensor $\bar{\tau}$ is,

$$\vec{\tau} = \mu_l \left[\nabla \vec{u}_l + \nabla \vec{u}_l^T \right] - \frac{2}{3} \nabla \bullet \vec{u}_l I \tag{3}$$

μ_l (Pa s) is the blood molecular viscosity; I the unit tensor and the second term in the right hand side is the effect of the volume dilation. The blood was considered to be non-Newtonian fluid obeying to the power law [23,24]. According to this law the molecular viscosity, now denoted as $\mu_l(\dot{S})$,

$$\mu_l \left(\dot{S} \right) = k e^{\frac{T_o}{T}} \dot{S}^{n-1} \tag{4}$$

$\dot{S}$ (1/s) is the shear rate,

$$\dot{S} = \frac{\partial u_{i,l}}{\partial x_{j,l}} + \frac{\partial u_{j,l}}{\partial x_{i,l}} \tag{5}$$

The consistency index k is set 0.00622 kg s^{n-2}/m; the power-law index n is 0.7, T (K) and T_o (K) are local and reference temperatures, respectively. The actual shear stress τ (N/m^2) is,

$$\tau = \left[\eta \left(\dot{S} \right) \right] \dot{S} \tag{6}$$

Arterial wall flow: Intima: The transmural flow through the intima layer is described by Darcy's Law,

$$\bar{u}_w = \frac{k_p^{in}}{\mu_p} \nabla \left(p_w \right) \tag{7}$$

$$\nabla \bullet \bar{u}_w = 0 \tag{8}$$

$\bar{u}_w$ (m/s) is the velocity vector within the intima layer or else the transmural velocity; k_p^{in} (m^2) is the Darcy's intima permeability coefficient, μ_p (Pa s) the blood plasma molecular (dynamic) viscosity having different viscosity than lumen blood and p_w (N/m^2) the pressure within the intima layer.

Media: The transmural flow through the media layer is described by Darcy's Law,

$$\overline{u}_w = \frac{k_p^m}{\mu_p}\nabla\left(p_w\right) \tag{9}$$

$$\nabla\bullet\overline{u}_w = 0 \tag{10}$$

k_p^m (m²) is the Darcy's media permeability coefficient and p_w (N/m²) the pressure within the media layer.

Mass transport equations

Lumen mass: The convection-diffusion equation for the lumen is,

$$\nabla\bullet\left(\overline{u}_l C_l\right) = D_l\nabla^2 C_l \tag{11}$$

$\overline{u}_l$ (m/s) is the lumen velocity vector, C_l (gr/l) is the LDL concentration and D_l (m²/s) is the solute diffusion coefficient in the lumen.

Arterial wall mass: The LDL concentration equation through the multi-layer intima and media arterial wall is introduced,

$$\mathrm{K}'_{lag}\,\overline{u}_w\forall c_w = D_{eff}^{in}\Delta c_w \tag{12}$$

$$\mathrm{K}'_{lag}\,\overline{u}_w\forall c_w = D_{eff}^{m}\Delta c_w - r_w c_w \tag{13}$$

c_w (gr/l) is the solute concentration in the arterial wall; D_{eff}^{in} (m²/s) the effective diffusivity in the intima layer; D_{eff}^{m} (m²/s) the effective diffusivity in the media layer; K'_{lag} the solute lag coefficient and r_w the constant consumption rate.

Flow boundary conditions

Lumen flow: A parabolic velocity inlet profile is applied,

$$u_0 = U_{in}\left(1-\left(\frac{R}{R_l}\right)^2\right) \tag{14}$$

U_{in} (m/s) is the instantaneous velocity applied into the lumen entrance, R (m) is the radial location from the centerline and R_l (m) the lumen radius. The corresponding pulse wave is shown in figure 3 [25].

Multi-layered arterial wall: Inlet and outlet boundary surfaces for the intima analysis are considered to be the endothelium surface and the IEL respectively, whereas inlet and outlet boundary surfaces for the media layer analysis are considered to be the IEL surface and the end surface of media layer (adventitia), respectively. The transmural pressure i.e. the pressure difference between lumen and adventitia, is set at 70.0 mmHg. The intraluminal pressure is set at 87.5 mmHg with a media-adventitia constant pressure at 17.5 mmHg. The interfacial coupling between lumen-intima (endothelium) and intima-media (IEL) is achieved by the Kedem-Katchalsky Eqs. 18, 19 and Eqs. 24, 25 respectively. A Dirichlet boundary condition $C_w/C_0 = 0$ is set at the media-adventitia interface assuming that the transport of LDL from the adventitia to media and vice versa is zero [11]. It has been demonstrated that the effect of several different types of media-adventitia boundary conditions on the species distribution within the intima, IEL and media layers is negligible [26].

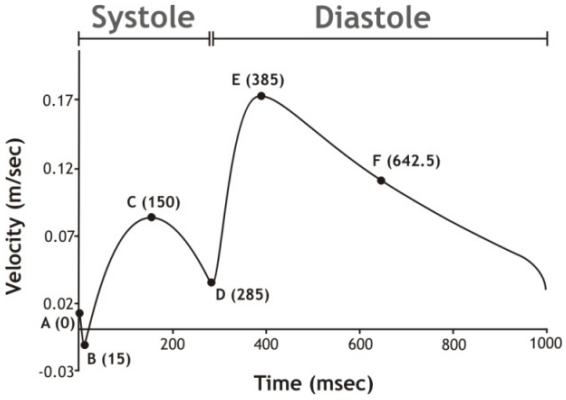

Figure 3: The pulse wave LCA segment form i.e. velocity (m/s) versus time (ms), for resting flow conditions is applied at lumen inlet.

AWSS: The time-averaged Wall Shear Stress (AWSS) (N/m²) magnitude is defined as,

$$AWSS = \frac{1}{T}\int_o^T\left|\vec{WSS}\right|dt \tag{15}$$

$\left|\vec{WSS}\right|$ (N/m²) is the instantaneous WSS magnitude; T (s) is the pulse period.

Mass transport boundary conditions

Lumen mass boundary conditions: A uniform constant concentration C_o of LDL (=1.3 gr/l) is set at the lumen left coronary orifice. At the segment outlet, the gradient of LDL concentration along the vessel is set to zero i.e. $\frac{\partial C_l}{\partial s}=0$. The applied endothelium boundary condition is,

$$\overline{C}_l^{\,end}J_v^{end} - D_l\frac{\partial\overline{C}_l^{\,end}}{\partial n} = \overline{C}_l^{\,end}\left[D_{eff}^{\prime,end} + J_v^{end}\left(1-\sigma_f^{end}\right)\right] \tag{16}$$

J_v^{end} (m/s) is the volume flux across the endothelium; n is the direction normal to endothelium (wall); D_{eff}^{end} (=6.0×10^{-17} m²/s [8]) is the effective endothelial diffusivity, thus the endothelial diffusive permeability $D_{eff}^{\prime,end}$ is 3.0×10^{-11} m/s per unit length and σ_f^{end} is the endothelial reflection coefficient (=0.9890 [9]). The time-averaged luminal surface concentration of LDL (gr/l) $\overline{C}_l^{\,end}$ is defined as,

$$\overline{C}_l^{\,end} = \frac{1}{T}\int_o^T C_{l,in}^{end}\,dt \tag{17}$$

$C_{l,in}^{end}$ (gr/l) is the instantaneous LDL at the lumen/endothelium interface. The LDL concentration values are averaged over the entire pulse period at each computational grid node of the endothelium.

Lumen-media (endothelium) coupling

The interfacial coupling (lumen-media) via the endothelium is achieved by the Kedem-Katchalsky equation, [27-28],

$$J_v^{end} = L_p^{end}\left(\Delta p^{end} - \sigma_d^{end}\Delta\pi^{end}\right) \tag{18}$$

$$J_s^{end} = D_{eff}^{\prime,end}\left(\Delta\overline{C}^{end}\right) + J_v^{end}\left(1-\sigma_f^{end}\right)\overline{C}_l^{\,end} \tag{19}$$

L_p^{end} (m²s/Kg) is the endothelium hydraulic conductivity; Δp^{end} (N/m²) the pressure drop across the endothelium; σ_d^{end} the osmotic reflection coefficient of the endothelium; $\Delta\pi^{end}$ (N/m²) the osmotic pressure difference across the endothelium; J_s^{end} ($\frac{gr}{l}\cdot\frac{m}{s}$) the solute

flux and $\Delta\overline{C}^{end}$ (gr/l) the LDL concentration difference across the endothelium $(\overline{C_l}^{end} - C_w^{end})$. The osmotic pressure difference $\Delta\pi^{end}$ is neglected to decouple the fluid dynamics from the solute dynamics [21]. Therefore, assuming $\Delta\pi^{end}$ is zero, the Eq. 18 can be written,

$$J_v^{end} = L_p^{end} \Delta p^{end} \tag{20}$$

In the present study, the parameters J_v^{end} and Δp^{end} need to be estimated. The procedure sets values to J_v^{end} so that the value of Δp^{end} has to be close to that used by Mpairaktaris et al. [6] (=16.0 mmHg). The procedure starts with the principle that the arterial wall is variable and the thickness ranges from 0.12 mm to 0.39 mm. This implies that the J_v^{end} value is in the range of 5.0×10^{-8}-1.5×10^{-7} m/s, which is clearly higher than the literature values, 1.5×10^{-8} -2.05×10^{-8} m/s [7]. This is justified as follows: Δp^{end}, following the procedure reported in Prosi et al. [18], is calculated, solving the following three equations,

$$R_{tot} = \frac{\Delta p^{(end+in+iel+m)}}{J_v^{end}} \tag{21}$$

$$R_{tot} = R^{end} + R^{in} + R^{iel} + R^{m} = \frac{1}{L_p^{end}} + \frac{\mu_p . L''^{in}}{K_p^{in}} + \frac{1}{L_p^{iel}} + \frac{\mu_p . L''^{m}}{K_p^{m}} \tag{22}$$

$$\Delta p^{end} = \frac{J_v^{end}}{L_p^{end}} \tag{23}$$

R_{tot} (Kg/m²s) is the total resistance of the arterial wall; $\Delta p^{(end+in+iel+m)}$ $(=p_l - p_{adv}$ =70.0 mmHg) is the pressure drop across the arterial wall; R^{end}, , R^{in}, , R^{iel}, , R^{m} are the resistances of the endothelium layer; intima layer; IEL and media layer, respectively; L''^{in} ($=0.012\times10^{-3}$ m close to the value proposed by Chung & Vafai, 2014 [30]) is the thickness of the intima layer; L''^{m} ($=0.24\times10^{-3}$ m) is the average thickness of the media layer. Solving the above system of linear equations with three unknowns (Δp^{end}, J_v^{end}, L_p^{end}) by setting L''^{m} = 0.12 mm, the J_v^{end} is 1.5×10^{-7} m/s whereas by setting L''^{m} = 0.39 mm, the J_v^{end} is 5.0×10^{-8}. For simplicity, we assume an average value L''^{m} =0.24 mm. Then, J_v^{end} is 8.0×10^{-8} m/s, Δp^{end} =16.17 mmHg and L_p^{end} =3.712 $\times10^{-11}$ $\frac{m^2.s}{Kg}$.

Intima-media (internal elastic layer coupling)

Similarly, the interfacial coupling between intima and media layer (IEL) is achieved,

$$J_v^{iel} = L_p^{iel}\left(\Delta p^{iel} - \sigma_d^{iel}\Delta\pi^{iel}\right) \tag{24}$$

$$J_s^{iel} = D'^{,iel}_{eff}\left(\Delta C^{iel}\right) + J_v^{iel}\left(1-\sigma_f^{iel}\right)C^{iel} \tag{25}$$

J_v^{Iel} (=7.8×10⁻⁸ m/s) is the volume flux across IEL; L_p^{Iel} (mm²s/gr) the IEL hydraulic conductivity; Δp^{Iel} (N/m²) the pressure drop across the IEL; σ_d^{Iel} the osmotic reflection coefficient; $\Delta\pi^{Iel}$ (N/m²) the osmotic pressure difference across IEL; J_s^{Iel} the solute flux; D_{eff}^{iel} (=1.066×10⁻⁸ mm²/s [9]) the effective diffusivity of internal elastic layer, thus the IEL diffusive permeability $D'^{,iel}_{eff}$ is equal to 0.533×10^{-8} m/s per unit length, close to the value 1.6×10^{-8} m/s used by Sun et al. [15]; ΔC^{Iel} (gr/l) the LDL concentration difference across IEL and σ_f^{iel} (=0.9827 [11]) the solvent reflection coefficient of the IEL.

Solving equation,

$$L_p^{iel} = \frac{K_p^{iel}}{\mu_p \bullet L''^{in}} \tag{26}$$

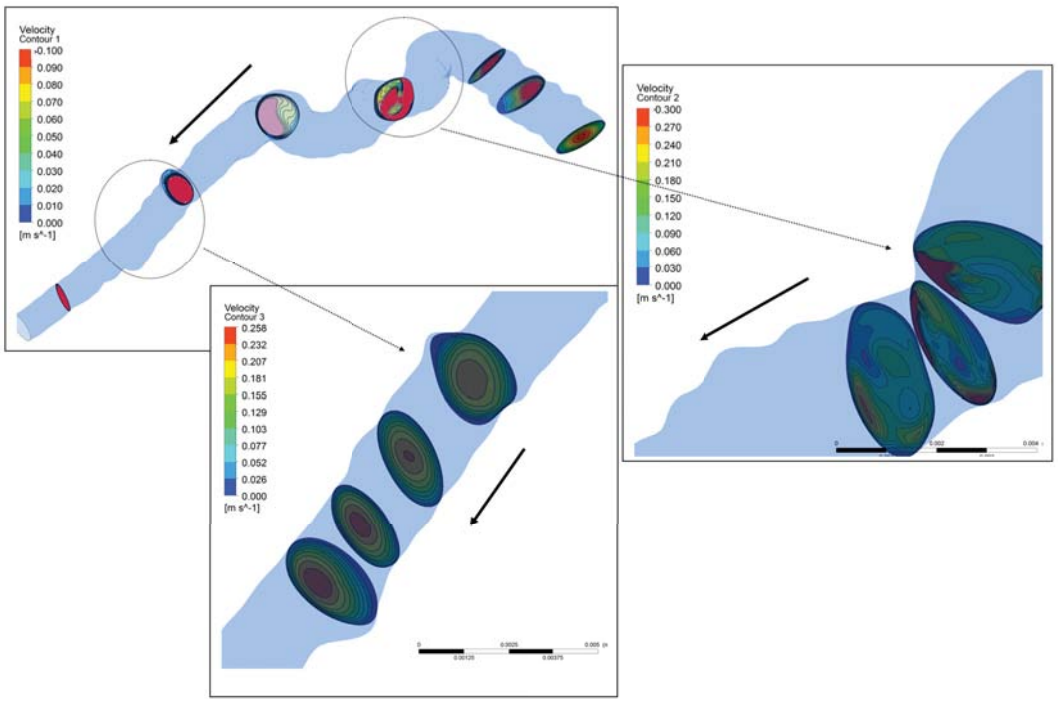

Figure 4: Blood velocity magnitude (m/s) contours at various LCA segment cross-sections.

ISSN: 2639-3786

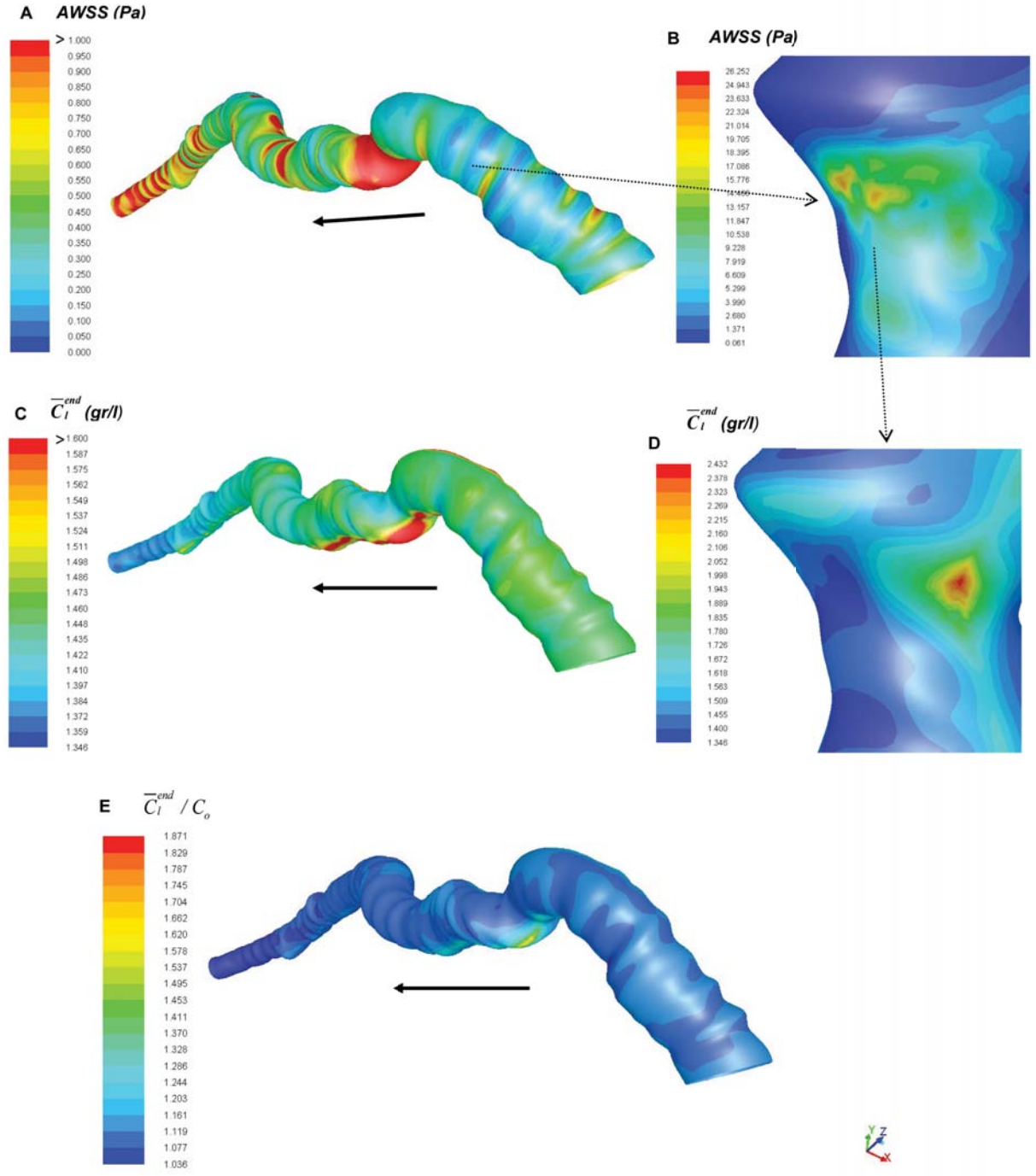

Figure 5: Contours over the LCA luminal surfaces.
A. AWSS (Pa); B. AWSS (Pa), enlarged view; C. Time-averaged LDL concentration $\overline{C}_l^{end}$ (gr/l); D. $\overline{C}_l^{end}$ (gr/l), enlarged view; E. Time-averaged normalized LDL concentration $\overline{C}_l^{end} / Co$

the hydraulic conductivity L_p^{Iel} is equal to 3.05×10^{-10} $\frac{m^2.s}{Kg}$. According to Chung & Vafai; Ai & Vafai; Chung & Vafai [12,17,29] the filtration velocity has been reported to be of the order ~ 10^{-8} m/s. The filtration velocity is almost unchanged across the arterial wall. Thus, we assume that J_v^{Iel} is 7.8×10^{-8} m/s. Thereafter, solving Eq. 24 for IEL, Δp^{iel} =1.918 mmHg.

Lumen and arterial wall physical parameters

The blood density ρ is set to 1058.0 kg/m^3 and the dynamic viscosity μ_p is 0.72×10^{-3} Pa s [11,16,19,30].

The Darcy permeability K_p^m is 2.0×10^{-18} m^2 [11,16,19,30] for the media layer; K_p^{in} is 2.0×10^{-16} m^2 [10] for the intima layer; K_p^{iel} is 4.392×10^{-19} m^2 [10] for IEL.

The solute lag coefficient K'_{lag} is $(1-\sigma_f^m = 0.1164)$ for the media layer and $(1-\sigma_f^{in} = 0.1728)$ for the intima layer [11]; the porosity ε 0.258 [9,11,16,19] for the media layer and 0.983 [11] for the intima layer.

The D_l is isotropic 2.867×10^{-11} m²/s [11,14]; the D_{in} 5.4×10^{-12} m²/s [10,16,19,29] and the D_m 5×10^{-14} m²/s [10,16, 19,29].

The $L^{\prime\prime end}$ 2.0×10^{-6} m [30]; the $L^{\prime\prime iel}$ 2.0×10^{-6} m [30] and the constant consumption rate inside the media layer is r_w=-3.197x10^{-4} 1/s and zero in other layers [11,12].

RESULTS

WSS and LDL transport in lumen

The AWSS and LDL transport in the lumen of LCA arterial wall was computationally analyzed under 70.0 mmHg transmural pressure. Figure 4 shows the blood velocity magnitude (m/s) at various arterial cross-sections. Velocity magnitudes of ~ 1.0 m/s are reached in the region within shape "S" formation. The flow pattern, which is affected from geometry abnormality, plays a significant role in the LDL distribution at the luminal interface.

The AWSS N/m² contours using non-Newtonian Power Law model over the LCA endothelial surfaces are shown in figure 5A and figure 5B (enlarged view). Concave parts exhibit primarily low AWSS. However, some convex parts may exhibit low AWSS as well. The time-averaged luminal surface LDL concentration $\overline{C}_l^{end}$ (gr/l) is shown in Figure 5C and Figure 5D (enlarged view). The normalized $\overline{C}_l^{end}/C_o$ concentration at the luminal side is shown in Figure 5E. Values $\overline{C}_l^{end}/C_o > 1.0$ indicate concentration polarization. The peak concentration of $\overline{C}_l^{end}$ =2.432 gr/l is 86.92 % higher than that at entrance and it is noticeable at concave parts of the region (shape "S"). Increased time-averaged luminal concentration values develop mainly at the last three quarters of the segment. Figure 6A shows that high LDL is located mainly at regions where AWSS ranges between 0.20 N/m² and 0.40 N/m². However, high LDL covers larger areas compared to the areas covered by low AWSS indicating that AWSS is not the only physical parameter affecting LDL distribution.

LDL transport in the intima layer

Figure 6B focuses on the AWSS <1.0 Pa variation with $\overline{C}_w^{in}/Co$. Figure 7A illustrates the LDL concentration $\overline{C}_w^{in}/Co$ at the endothelium/intima interface. The $\overline{C}_w^{in}/Co$ values are lower to the corresponding ones at the lumen side (~ order of 10^{-2}). High $\overline{C}_w^{in}/Co$ nearly coincides with high luminal surface concentration. Figure 7B depicts an enlarged view of the region within shape "S" formation. The peak concentration is 0.0213, which is higher than LDL occuring

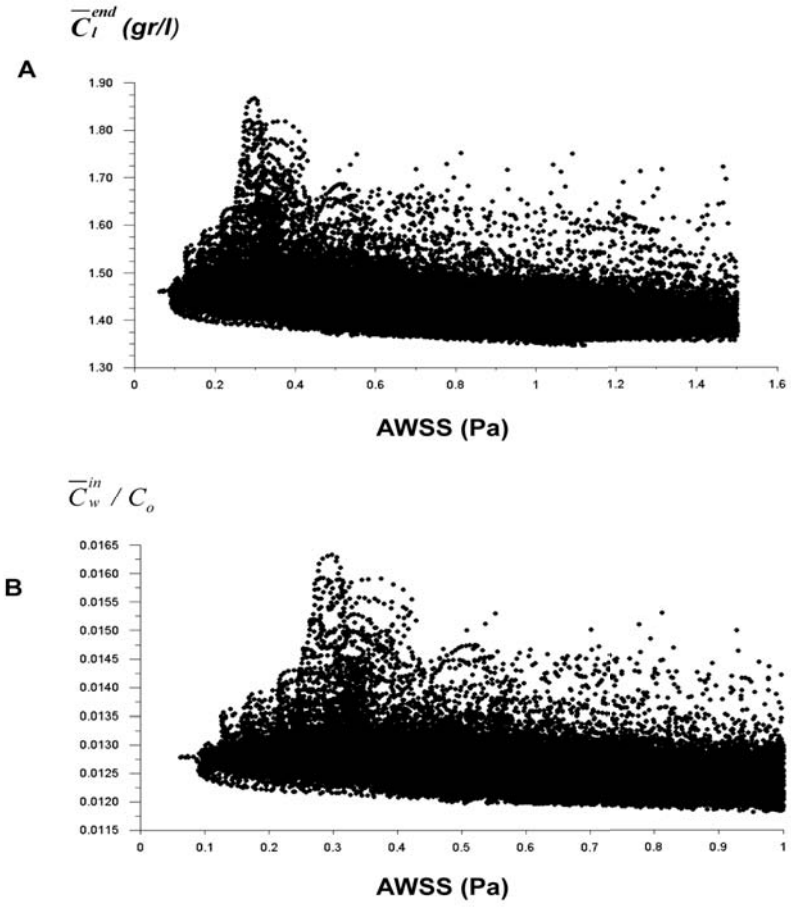

Figure 6: A. $\overline{C}_l^{end}$ (gr/l) versus AWSS (Pa) from 0.0 to 1.5 Pa range over the LCA luminal endothelium surface
B. $\overline{C}_w^{in}/Co$ versus AWSS (Pa) from 0.0 to 1.0 Pa range at the endothelium-intima interface

ISSN: 2639-3786

at the endothelium/intima interface.

Figure 7C shows the $\overline{C}_w^{in} / Co$ variation with radial distance r at an arbitrary LCA cross-section. The concentration drop between endothelium and IEL along the distance r is negligible.

LDL transport in the media layer

Contours of normalized concentration $\overline{c}_w^{med} / Co$ within the arterial wall (media layer) at region adjacent to IEL are shown in figure 8A. Values of $\overline{c}_w^{med} / Co$ vary in the range of 0.00095 and 0.00168. The IEL prohibits mass transfer across it. Thus, the LDL concentration at the IEL/media interface is substantially reduced in comparison to intima layer.

Contours of $\overline{c}_w^{med} / Co$ concentration at 4 arbitrary chosen LCA arterial cross-sections are shown in figure 8B. An enlarged view of a specific cross-section is also shown (Figure 8C). The intima layer covers small rig area and is shown with yellow colour. The media layer is shown with green and blue colour zones. In this analysis, the very end of the media layer coincides with the very end of the adventitia layer where appropriate boundary conditions are specified.

Figure 8D shows the concentration $\overline{c}_w^{med} / Co$ across the media layer as a function of radial distance r at an arbitrary line (Figure 8C). The LDL concentration is nearly 0.001 at the IEL/media interface. The concentration reduces to 0.0 at a point located at the very end of the media layer (adventitia).

LDL transport along arterial wall cross-section

Figure 9 shows the LDL distribution $\overline{C}_w / C_o$ across a typical cross-section of the multi-layer arterial wall. Increased concentration, as high as 0.0124, occurs in the intima layer. The IEL drastically reduces the concentration as it acts as a "buffering region". LDL concentration values in the media layer are at least one order of magnitude smaller to those occurring at the endothelium-intima interface.

DISCUSSION

Atherosclerosis is relevant to distribution of LDL associated with the local intravascular rheological conditions. Furthermore, the patient-specific vascular geometries are associated with the LDL transport at the vascular wall layers.

The main objective of this study was to simulate the LDL transport and its distribution within the patient-specific arterial wall under unsteady flow conditions assuming the arterial wall to be composed of non-homogeneous porous media. The model was simulated assuming the blood being of non-Newtonian fluid with constant diffusivity. The specific difference between Newtonian and Non-Newtonian blood flow with constant diffusivity is the WSS magnitude [31]. They reported that, using Newtonian model, the maximum WSS values are ~100.0% higher to those using the non-Newtonian power model. On the contrary, they also reported that the spatial and temporal distribution WSS patterns are barely affected. The primary sources of parameters for the current analysis came

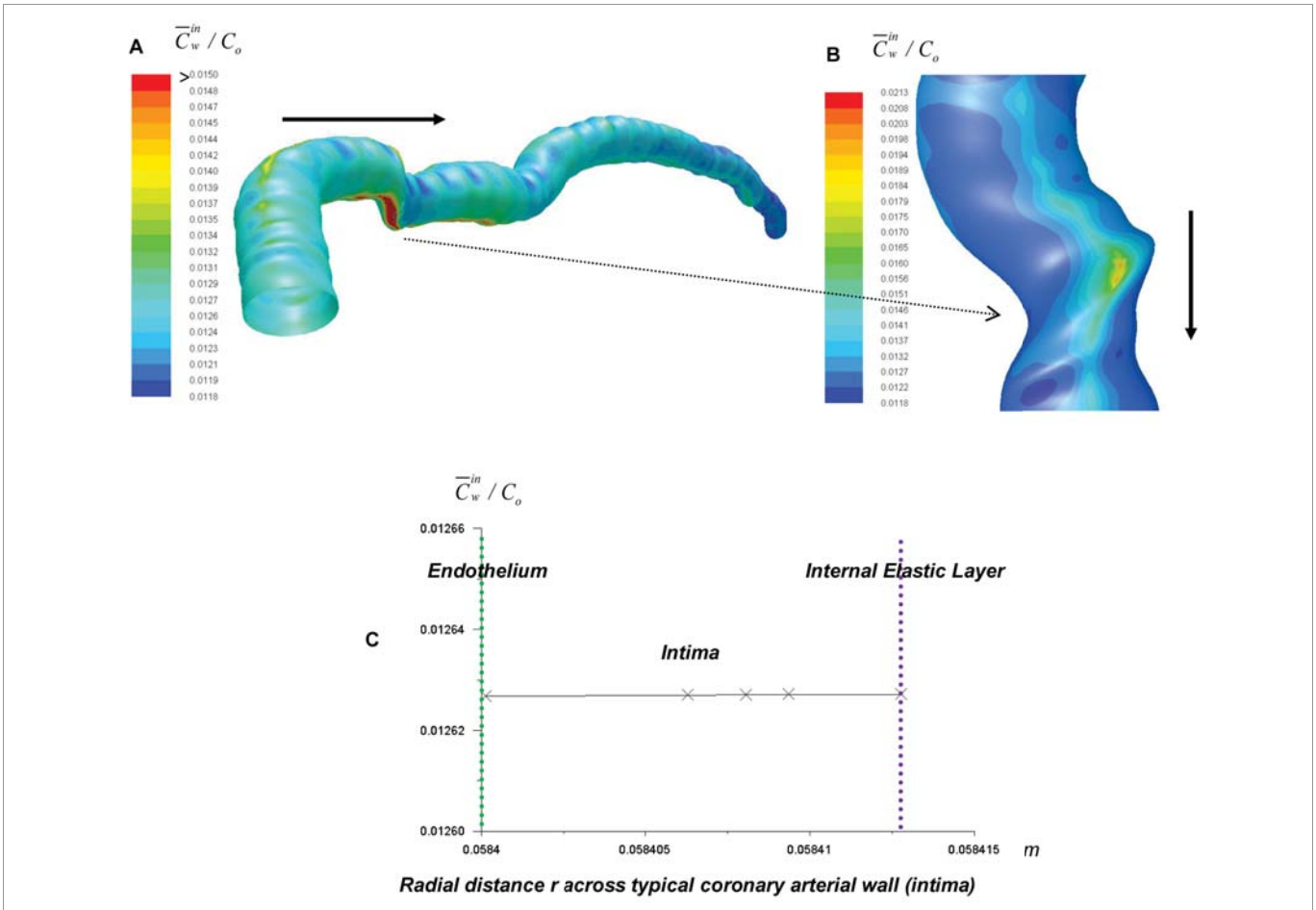

Figure 7: A. Time-averaged normalized concentration $\overline{C}_w^{in} / Co$ over intima at region adjacent to endothelium B. $\overline{C}_w^{in} / Co$, enlarged view and C) normalized $\overline{C}_w^{in} / Co$ concentration variation along intima radial distance r at an arbitrary LCA cross-section.

ISSN: 2639-3786

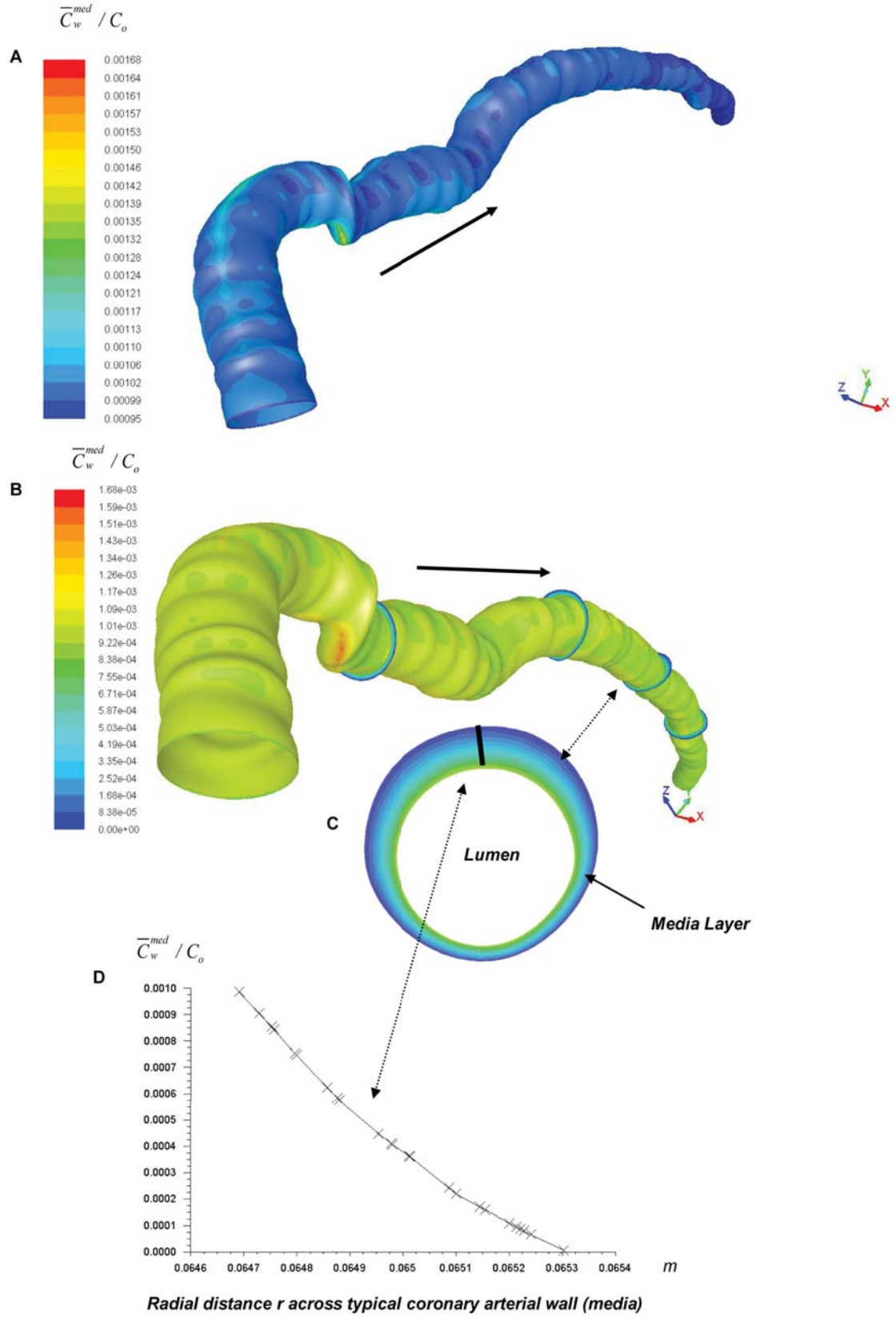

Figure 8: A. Contours of normalized $\overline{C}_w^{med} / Co$ concentration within the arterial wall (media layer) at region adjacent to IEL
B. contours of normalized $\overline{C}_w^{med} / Co$ concentration at 4 arbitrary chosen LCA arterial cross-sections within media layer
C. contours of normalized $\overline{C}_w^{med} / Co$ concentration within an arbitrary chosen cross-section, enlarged view
D. normalized $\overline{C}_w^{med} / Co$ concentration across the media layer as a function of radial distance r at an arbitrary line

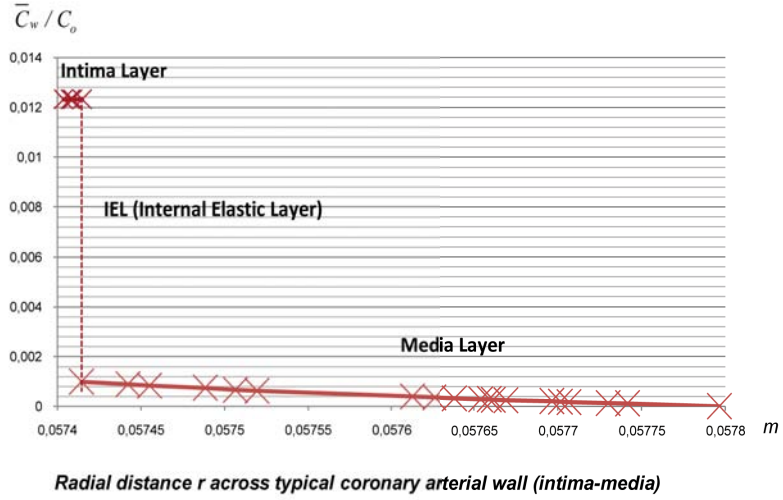

Figure 9: Normalized $\bar{C}_w / Co$ concentration along a typical cross-section of the multi-layer arterial wall.

mainly from Wang & Vafai [11], Kenjeres et de Loor [19], Chung & Vafai [30]. The computational approach is similar to that proposed by Sun et al. [14] and Sun et al. [15].

A crucial assumption was made about the WSS. This states that the WSS does not simultaneously and directly affect the endothelial cells. This implies that the characteristic time of endothelial cell response to shear stress is much longer than that of WSS oscillation [7,32]. Thus, the WSS values were averaged over the entire pulse period for each computational grid node adjacent to the endothelium. Moreover, considering that the LDL effects upon endothelial permeability take place with time delay, we assume that the time-dependent LDL must be averaged over the entire pulse period. Otherwise, substantial error could be introduced in spotting the prone to atherosclerosis arterial wall regions.

Current results indicate that the LDL concentration at the lumen-endothelium interface ranges from 1.3 gr/l to 2.43 gr/l. This implies that the peak concentration is 86.92 % higher than that at the entrance. Moreover, the lumen-side LDL concentration occurs preferably at the concave geometry parts denoting concentration polarization. The AWSS distribution has an inverse relation to the luminal surface LDL concentration. However, some convex parts may exhibit low AWSS and some concave parts may exhibit high AWSS. Geometry abnormalities, within shape "S" formation, affect the flow pattern, changing it from stable to unstable due to the development of complex secondary and recirculation flows. This fact plays significant role in the LDL distribution at the luminal side as well as within the arterial wall. Therefore, within this formation, not only concave parts are associated with very low AWSS coinciding with high LDL concentration, but some nearby curved parts coincide with high LDL levels although the AWSS is relatively elevated. This state is coherent with the results of Olgac et al. [7]. Consequently, WSS is not the only factor that determines the LDL distribution [6]. It is also remarkable that the increased time-averaged luminal concentration develops mainly in the proximal rather than to distal direction. This result is in good agreement with Olgac et al. [33] and it may be attributed to the flow momentum loss from proximal to distal segment regions.

On the other hand, high LDL concentration at the endothelium/intima interface nearly coincides with high luminal surface concentration and low AWSS. The LDL accumulation in the arterial intima is a critical step in the initiation and progression of atheromatous lesions. Specifically, the intimal hyperplasia which is the "migration" result of Smooth Muscle Cells (SMCs) from media to intima, (the hypertension gives a further boost to that process [26]) incorporates LDL transportation and accumulation. In recent computational studies, the process of plaque formation is modeled assuming LDL oxidation modeling and intima-media thickness analysis [34]. Current results indicate that the LDL at the endothelium/intima interface is substantially lower, almost 90 times, than its value at lumen/endothelium interface. In comparison to our previous study [6], the LDL at the endothelium/media interface was lower 20 times than the corresponding luminal (endothelium side) concentration for the tested patient-specific thoracic arterial wall. This fact may be attributed to the differential volume flux calculation formula incorporating the local wall thickness. This, also, means that the local geometric characteristics, such as the thickness of the arterial wall and the total resistance of the artery, determine the volume flux value affecting the LDL accumulation within the arterial wall. Thus, the simplification of simulating an idealize artery with constant thickness can lead to underestimation of the wall thickness influence to the volume flux. However, our results are in general agreement with relevant studies [10-13,15,17].

Our results indicate that the LDL concentration drop across the intima layer is negligible due to the extremely low thickness of the porous media which is coherent with the results in general literature [10,11,17,35]. The LDL concentration reduction across the IEL is remarkable. As it was mentioned above, the IEL acts as a "buffering region". Therefore, LDL concentration values at the IEL/media interface are one order of magnitude smaller to ones occurring at the intima layer. Within the media layer, the LDL concentration is further reduced towards media-adventitia arterial wall forming a curved line due to the constant consumption rate. At the very end of the media layer (adventitia), the LDL reduces to zero because of the applied boundary condition.

In future research work, the arterial wall could be treated as flexible while the permeability of endothelium could be WSS dependent. Additional effort is needed to simulate the accurate thickness of the intima porous layer. This factor could provide more specific results.

CONCLUSION

A relationship between AWSS, LDL concentration at the luminal side and its concentration within the multi-layer arterial wall was

examined under pulsatile flow for a patient-specific LCA. This model takes into account the instantaneous LDL for the calculation of the average LDL concentration. Results showed that LDL across the arterial wall varies within layers and high LDL occurs, almost, in regions of high luminal side (endothelium) LDL concentration. The endothelium layer and the IEL prohibit substantial LDL transport to the intima and media respectively. The transportation of LDL through the multilayer arterial wall is affected by the flow pattern itself and the thickness of the arterial wall.

REFERENCES

1. Mozaffarian D, Benjamin EJ, Go AS, Arnett DK, Blaha MJ, Cushman M, et al. Heart disease and stroke statistics--2016 update: a report from the American Heart Association. Circulation. 2016; 133 :e38-360. https://goo.gl/ADYk2W
2. Wada S, Karino T. Theoritical prediction of low-Density lipoproteins concentration at the luminal surface of an artery with a multiple bend. Ann Biomed Eng. 2002; 30: 778-791. https://goo.gl/iSHtTn
3. Chatzizisis YS, Jonas M, Coskun AU, Beigel R, Stone BV, Maynard C, et al. Prediction of the localization of High-Risk coronary Atherosclerotic plaques on the basis of low endothelial shear stress: an intravascular ultrasound and histopathology natural history study. Journal of the american heart association. Circulation. 2008; 117: 993-1002. https://goo.gl/eZV5aN
4. Huo Y, Wischgoll T, Kassab GS. Flow patterns in three-dimensional porcine epicardial coronary arterial tree. Am J Physiol Heart Circ Physiol. 2007; 293: H2959-2970. https://goo.gl/11JXZZ
5. Zhang JM, Zhong L, Su B, Wan M, Yap JS, Tham JP, et al. Perspective on CFD studies of coronary artery disease lesions and hemodynamics: A review. Int J Numer Method Biomed Eng. 2014; 30: 659-680. https://goo.gl/Ber8tR
6. Mpairaktaris DG, Soulis JV, Giannoglou GD. Low density lipoprotein transport through patient-specific thoracic arterial wall. Comput Biol Med. 2017; 89: 115-126. https://goo.gl/2Y2ens
7. Olgac U, Poulikakos D, Saur SC, Alkadhi H, Kurtcuoglu V. Patient-specific three-dimensional simulation of LDL accumulation in a human left coronary artery in its healthy and atherosclerotic states. Am J Physiol Heart Circ Physiol. 2009; 296: H1969-1982. https://goo.gl/1WeJTT
8. Iasiello M, Vafai K, Andreozzi A, Bianco N. Low-density lipoprotein transport through an arterial wall under hyperthermia and hypertension conditions–An analytical solution. J Biomech. 2016; 49: 193-204. https://goo.gl/4mZUo4
9. Jesionek K, Slapik A, Kostur M. Effect of hypertension on low-density lipoprotein transport within a multi-layered arterial wall: modelling consistent with experiments. ArXiv: 1604.03735v1; 1-19. https://goo.gl/vheTT3
10. Iasiello M, Vafai K, Andreozzi A, Bianco N, Tavakkoli F. Effects of external and internal hyperthermia on LDL transport and accumulation within an arterial wall in the presence of a stenosis. Ann Biomed Eng. 2015; 43: 1585-1599. https://goo.gl/bLB69H
11. Wang S, Vafai K. Analysis of Low Density Lipoprotein (LDL) Transport Within a Curved Artery. Ann Biomed Eng. 2015; 43: 1571-1584. https://goo.gl/6jkPVe
12. Chung S, Vafai K. Low-density lipoprotein transport within a multi-layered arterial wall-Effect of the atherosclerotic plaque/stenosis. J Biomech. 2013; 46: 574-585. https://goo.gl/yPY4YZ
13. Khakpour M, Vafai K. A comprehensive analytical solution of macromolecular transport within an artery. International Journal of Heat and Mass Transfer. 2018; 51: 2905-2913. https://goo.gl/Md3F3x
14. Sun N, Wood NB, Hughes AD, Thom SA, Xu XY. Influence of pulsatile flow on LDL transport in the arterial wall. Ann Biomed Eng. 2007; 35: 1782-1790. https://goo.gl/nCCFXm
15. Sun N, Wood NB, Hughes AD, Thom SA, Yun Xu X. Effects of transmural pressure and wall shear stress on LDL accumulation in the arterial wall: a numerical study using a multilayered model. Am J Physiol Heart Circ Physiol. 2007; 292: H3148-H3157. https://goo.gl/LC3k2s
16. Yang N, Vafai K. Modeling of Low-Density Lipoprotein (LDL) transport in the artery-effects of hypertension. International Journal of Heat and Mass Transfer. 2006; 49: 850-867. https://goo.gl/s28ekZs
17. Ai L, VafaiK. A coupling model for macromolecule transport in a stenosed arterial wall. International Journal of Heat and Mass Transfer. 2006; 49: 1568-1591. https://goo.gl/Mvjbr3
18. Prosi M, Zunino P, Perktold K, Quarteroni A. Mathematical and numerical models for transfer of low-density lipoproteins through the arterial walls: a new methodology for the model set up with applications to the study of disturbed lumenal flow. J Biomech. 2005; 38: 903-917. https://goo.gl/4n9mSF
19. Kenjereš S, de Loor A. Modelling and simulation of low-density lipoprotein transport through multilayered wall of an anatomically realistic carotid artery bifurcation. J R Soc Interface. 2013; 11: 20130941. https://goo.gl/j832AD
20. Sakellarios AI, Papafaklis MI, Siogkas P, Athanasiou LS, Exarchos TP, Stefanou K, et al. Patient-specific computational modeling of subendothelial LDL accumulation in a stenosed right coronary artery: effect of hemodynamic and biological factors. Am J Physiol Heart Circ Physiol. 2013; 304: H1455-H1470. https://goo.gl/Kqtoso
21. Olgac U, Kurtcuoglu V, Poulikakos D. Computational modeling of coupled blood-wall mass transport of LDL: effects of local wall shear stress. Am J Physiol Heart Circ Physiol. 2008; 294: H909-H919. https://goo.gl/QU3Q5U
22. Doulaverakis C, Tsampoulatidis I, Antoniadis AP, Chatzizisis YS, Giannopoulos A, Kompatsiaris I, et al. IVUS Angio tool: a publicly available software for fast and accurate 3D reconstruction of coronary arteries. Comput Biol Med. 2013; 43: 1793-1803. https://goo.gl/oBFE3M
23. Soulis JV, Fytanidis DK, Papaioannou VC, Giannoglou GD. Wall shear stress on LDL accumulation in human RCAs. Med Eng Phys. 2010; 32: 867-877. https://goo.gl/gP535ms
24. Sharma K, Bhat SV. Non-Newtonian rheology of leukemic blood and plasma: are n and k parameters of power law model diagnostic?. Physiol Chem Phys Med NMR. 1992; 24: 307-312. https://goo.gl/cfwGYX
25. Nosovitsky VA, Ilegbusi OJ, Jiang J, Stone PH, Feldman CL. Effects of curvature and stenosis-like narrowing on wall shear stress in a coronary artery model with phasic flow. Comput Biomed Res. 1997;30: 61-82. https://goo.gl/rE8vQ5
26. Dabagh M, Jalali P, Tarbell JM. The transport of LDL across the deformable arterial wall: the effect of endothelial cell turnover and intimal deformation under hypertension. Am J Physiol Heart Circ Physiol. 2009; 297: H983-H996. https://goo.gl/N1WFG2
27. Katchalsky A, Curran P. Nonequilibrium thermodynamics in biophysics. Harvard University Press. Cambridge MA. 1981.
28. Kedem O, Katchalsky A. Thermodynamic analysis of the permeabilityof biological membranes to non-electrolytes. Biochimica et Biophysica Acta. 1958; 27: 229-246. https://goo.gl/ZQQGST
29. Chung S, Vafai K. Effect of the fluid-structure interactions on low-density lipoprotein transport within a multi-layered arterial wall. J Biomech. 2012; 45: 371-381. https://goo.gl/K6RJTLs
30. Chung S, Vafai K. Mechanobiology of low-density lipoprotein transport within an arterial wall--impact of hyperthermia and coupling effects. J Biomech. 2014; 47: 137-147. https://goo.gl/4zXktv
31. Liu B, Tang D. Influence of Non-Newtonian properties of blood on the wall shear stress in human atherosclerotic right coronary arteries. Mol Cell Biomech. 2011; 8: 73-90. https://goo.gl/fPQq7ms
32. Sakamoto N, Ohashi T, Sato M. Effect of shear stress on permeability of vascular endothelial monolayer cocultured with smooth muscle cells. Jsme Int J C-Mech. 2004; 47: 992-999. https://goo.gl/3gpfpC
33. Olgac U, Knight J, Poulikakos D, Saur SC, Alkadhi H, Desbiolles LM, et al. Computed high concentrations of low-density lipoprotein correlate with plaque locationsin human coronary arteries. J Biomech. 2011; 44: 2466-2471. https://goo.gl/qrsV3w
34. Mirbagheri SA, Saidi MS, Sohrabi S, Firoozabadi B, Banazadeh MH. Effects of hypertension on Intima-Media Thickness (IMT); application to a human carotid artery, Scientia Iranica B. 2016; 23: 1731-1740.
35. Roustaei M, Nikmaneshi MR, Firoozabadi B. Simulation of Low Density Lipoprotein (LDL) permeation into multilayer coronary arterial wall: Interactive effects of wall shear stress and fluid-structure interaction in hypertension. J Biomech. 2018; 67: 114-122. https://goo.gl/9ohZxs